Journal of Power Sources 219 (2012) 133–139

Contents lists available at SciVerse ScienceDirect

Journal of Power Sources

journal homepage: www.elsevier.com/locate/jpowsour

One dimensional $La_{0.8}Sr_{0.2}Co_{0.2}Fe_{0.8}O_{3-\delta}/Ce_{0.8}Gd_{0.2}O_{1.9}$ nanocomposite cathodes for intermediate temperature solid oxide fuel cells

Erqing Zhao [a], Zheng Jia [a], Li Zhao [a], Yueping Xiong [a,*], Chunwen Sun [b,c], Manuel E. Brito [a,d]

[a] School of Chemical Engineering and Technology, Harbin Institute of Technology, 92 West Dazhi Street, Mailbox 1247, Harbin 150001, PR China
[b] Beijing National Laboratory for Condensed Matter Physics, Institute of Physics, Chinese Academy of Sciences, Beijing 100190, China
[c] Key Laboratory for Renewable Energy, Chinese Academy of Sciences, Beijing Key Laboratory for New Energy Materials and Devices, Beijing 100190, China
[d] Fuel Cell Material Group, Energy Technology Research Institute, National Institute of Advanced Industrial Science and Technology (AIST), Tsukuba 305-8565, Japan

HIGHLIGHTS

- The LSCF nanorods have been synthesized using an electrospinning method.
- Nanorod structured LSCF/GDC cathode was fabricated by an infiltration process.
- The obtained LSCF/GDC cathode has larger LSCF/GDC boundaries and higher porosity.
- The LSCF/GDC cathode has the lowest polarization resistance of 0.1 Ω cm^2 at 650°C.

ARTICLE INFO

Article history:
Received 5 May 2012
Received in revised form
4 July 2012
Accepted 6 July 2012
Available online 24 July 2012

Keywords:
$La_{0.8}Sr_{0.2}Co_{0.2}Fe_{0.8}O_{3-\delta}$
$Ce_{0.8}Gd_{0.2}O_{1.9}$
Composite cathode
Infiltrating
Electrospinning
Intermediate temperature solid oxide fuel cell

ABSTRACT

One dimensional $La_{0.8}Sr_{0.2}Co_{0.2}Fe_{0.8}O_{3-\delta}$ (LSCF) nanorod/$Ce_{0.8}Gd_{0.2}O_{1.9}$ (GDC) nanoparticle composite cathode has been fabricated by infiltrating the GDC precursor solution into LSFC scaffolds consisting of LSCF nanorods prepared with an electrospinning technique. For comparison, LSCF/GDC nanoparticle cathodes are also obtained using the same method. Impedance analysis reveals that nanorod structured LSCF/GDC cathode has a better electrochemical performance than that of the pure nanorod LSCF cathode, achieving a polarization resistance of 0.10 Ω cm^2 at 650 °C for the GDC loading of 160 μL, corresponding to about 50 wt.% GDC. Especially, the polarization resistance of nanorod LSCF/GDC cathode with 160 μL loading displays 5 times smaller than that of LSCF/GDC nanoparticle cathode with an optimal GDC loading of 80 μL at 650 °C, mainly due to its optimal structure with larger LSCF/GDC boundaries and higher porosity. These results imply that LSCF nanorod/GDC nanoparticle composite is a promising cathode material for intermediate temperature solid oxide fuel cell (IT-SOFC).

1. Introduction

SOFCs have attracted more and more attention because of their high energy conversion efficiency, less pollutant emissions and excellent fuel flexibility. Recently, significant efforts have been devoted to the development of SOFCs operating in the intermediate temperature range of 600 °C∼800 °C. Reducing the operating temperature of SOFCs can bring many benefits, such as lower cost, long operational life, and high selectivity of SOFC component materials. Unfortunately, the SOFC total resistance increases quickly as the operating temperature decreases. Electrolyte contribution to the total resistance can be controlled by designing anode supported SOFCs [1,2] or using a high oxygen ion conductor [3,4] under 600 °C∼800 °C operating conditions. The electrode polarization loss primarily originates from cathode polarization. However, perovskite-type $La_{1-x}Sr_xCo_{1-y}Fe_yO_{3-\delta}$ cathode has shown potential as an IT-SOFC cathode due to its high electrical and ionic mixed conductivities as well as excellent chemical and thermal stabilities [5–10].

For the pristine LSCF cathode, the O_2 reduction reaction is mainly confined to the electrode/electrolyte interface due to the lower ionic conductivity of LSCF (for $La_{0.8}Sr_{0.2}Co_{0.2}Fe_{0.8}O_3$, $\sigma_i = 2.2 \times 10^{-3}$ S cm^{-1}) [11], which results in low electro-catalytic activity of LSCF cathode for O_2 reduction reactions. The electro-catalytic activity of LSCF cathode can be further enhanced by adding oxygen ion conducting phases [12,13]. Recently, the infiltration method has been utilized to fabricate composite cathodes by

* Corresponding author. Tel.: +86 451 86413721; fax: +86 451 86418616.
E-mail address: ypxiong@hit.edu.cn (Y. Xiong).

0378-7753/$ – see front matter © 2012 Elsevier B.V. All rights reserved.
http://dx.doi.org/10.1016/j.jpowsour.2012.07.013

introducing an ion conductor phase or electron conductor phase into a pre-sintered porous backbone. Jiang et al. [14] studied the LSM/GDC composite cathode by a multi-step impregnation process, obtaining a polarization resistance of 0.72 Ω cm^2 compared to 26.4 Ω cm^2 of the blank LSM at 700 °C. Zhao et al. [15] fabricated $Sm_{0.5}Sr_{0.5}CoO_{3-\delta}/Sm_{0.2}Ce_{0.8}O_{1.9}$ composite cathodes with a nano-network by an ion-impregnation method for IT-SOFC, producing a polarization resistance of 0.21 Ω cm^2 at 500 °C, and 0.052 Ω cm^2 at 600 °C. Nie et al. [16] obtained the $La_{0.6}Sr_{0.4}Co_{0.2}Fe_{0.8}O_{3-\delta}/Sm_{0.2}Ce_{0.8}O_{1.95-\delta}$ composite cathode by infiltrating SDC into the LSCF scaffolds, achieving a polarization resistance of 0.4 Ω cm^2 at 650 °C, which is obviously lower than that of the pure LSCF cathode, indicating that the infiltration of the SDC phase significantly enhances the electro-catalytic activity of the LSCF electrodes for O_2 reduction reactions. Chen et al. [17] demonstrated that the infiltration of GDC into LSCF skeleton apparently reduced the LSCF cathode polarization resistance, achieving a polarization resistance of 1.6 Ω cm^2 for a GDC-infiltrated LSCF cathode compared to 5.4 Ω cm^2 for the blank LSCF cathode at 600 °C, showing that LSCF/GDC is a good candidate as an intermediate temperature SOFC cathode. Shah and Barnett [18] demonstrated that the infiltration of LSCF into porous GDC scaffolds pre-sintered on a GDC electrolyte substrate can decrease the LSCF sintering temperature and suppress the growth of LSCF particles so that the cathode polarization is alleviated. The lowest polarization resistance of 0.24 Ω cm^2 was measured at 600 °C.

Up to now, various processes have been explored to synthesize nanosized LSCF powders, such as polymer assisted combustion method [19–21], citrate complexion method [22–25] and dipping-pyrolysis method [26]. It is well known that the electrospinning technique is a very facile and effective approach to fabricate uniform nanofibers with small diameter, high specific area and porosity. In addition, this method also has other advantages, including low cost, simple apparatus, controllable process and extensive material sources. Azad [27] employed the elecrospinning technique to fabricate one dimensional (1D) YSZ and GDC fibers with a length of several inches from a polymeric solution containing appropriate metal cations. Li et al. [28] synthesized uniform YSZ nanofibers by electrospinning 8YSZ dispersion and applied it in a SOFC anode. Recently, the $La_{0.58}Sr_{0.4}Co_{0.2}Fe_{0.8}O_3$ nanofibers have been fabricated by the electrospinning technique and used as an intermediate temperature solid oxide fuel cell cathode [29]. To our knowledge, there are few reports on fabricating nanorod-structured LSCF/GDC composite cathodes for application in SOFC by the combination of the electrospinning and infiltration methods.

In this paper, we report a study on nanorod structured LSCF cathodes and GDC-infiltrated LSCF composites as cathodes for IT-SOFCs. One dimensional (1D) LSCF nanorods were fabricated by electrospinning with the LSCF precursor solution and applied as IT-SOFC cathodes. The electro-catalytic activity of LSCF cathode was significantly enhanced by infiltration of oxygen ion conducting phase GDC into LSCF scaffolds.

2. Experimental

$Ce_{0.8}Gd_{0.2}O_{1.9}$ (GDC) nanosized powders were synthesized using the citrate complexion method [30]. Then, electrolyte substrates were prepared by die pressing the as-synthesized GDC powder, followed by sintering at 1450 °C for 20 h in air. The substrate disks were 19 mm in diameter and 1.1 mm in thickness.

One dimensional LSCF/PVP nanofibers were obtained by electrospinning using $La(NO_3)_3\cdot 6H_2O$, $Sr(NO_3)_2$, $Co(NO_3)_2\cdot 6H_2O$, $Fe(NO_3)_3\cdot 9H_2O$, Polyvinylpyrrolidone (PVP) and *N*,*N*-dimethylformamide (DMF), followed by high temperature treatment at 900 °C for 2 h to form LSCF nanorods. In a typical synthesis, the above metal nitrates were dissolved in DMF in a molar ratio of La:Sr:Co:Fe = 0.8:0.2:0.2:0.8. Then a proper quantity of PVP was added into the as-prepared solution and stirred continuously for 4 h to get a homogeneous precursor solution for electrospinning. The appropriate LSCF precursor solution was loaded into a plastic syringe equipped with a flat stainless steel needle of 0.8 mm in diameter. A high voltage supply was connected to the spinneret (stainless steel needle) and a nickel mesh collector was placed 12 cm away from the orifice. The electric voltage was kept at 20 kV. The as-electrospun LSCF nanofibers were kept in air for 12 h to evaporate the solvent. Then, the dried LSCF nanofibers were calcined in the furnace at 900 °C for 2 h to form 1 D LSCF nanopowders. The metal composition of the obtained LSCF was determined by inductively coupled plasma atomic emission spectroscopy (ICP-AES) with an Optima 5300DV spectrometer. The microstructure and phase formation of LSCF were examined by scanning electron microscope (SEM, FEI Quanta 200, Holland) and X-ray diffraction (XRD, Rigaku D/max-IIB) using Cu Kα radiation, respectively.

Cathode pastes were prepared by dropping 3wt%-ethyl cellulose terpineol solution into LSCF nanorod powders, followed by magnetic stirring at ambient temperature for 12 h. Subsequently, the above as-prepared cathode pastes with LSCF nanorods were coated onto one side of the GDC electrolyte and calcined at 940 °C for 1 min with a heating rate of 15 °C min^{-1} in air to obtain the nanorod structured LSCF cathode with a weight of about 7 mg. As a comparison, the above LSCF nanorods were ground into LSCF nanoparticles by a mortar pestle. Then, the cathode stuff with LSCF nanoparticles was printed on one side of the GDC electrolyte and calcined at 1000 °C for 2 h to form a nanoparticle structured LSCF cathode with a weight of about 15 mg. The thickness of the LSCF cathode was about 60 um and the active electrode area was 0.785 cm^2.

According to the molecular formula $Ce_{0.2}Gd_{0.8}O_{1.9}$, the filtration solution of GDC precursor with a concentration of 0.25 mol L^{-1} was prepared by dissolving stoichiometric $Gd(NO_3)_3\cdot 6H_2O$ and $Ce(NO_3)_3\cdot 6H_2O$ in a mixed solvent of ethanol and deionized water. Infiltration was carried out by injecting the above nitrate aqueous solution of GDC precursor into the LSCF cathode pre-sintered on a GDC electrolyte using a microliter syringe to control the amount of GDC loading. To avoid leaking out of the edge of LSCF cathode, only 40 μL GDC precursor solution could be deposited once onto the LSCF cathode with nanorods, while only 20 μL for the LSCF cathode with nanoparticles. After each infiltration, the infiltrated LSCF cathode was dried in air and calcined at 700 °C for 30 min with a temperature gradient of 10 °C min^{-1}. The infiltration process was repeated to increase the GDC loading. Finally, the infiltrated electrode was fired at 800 °C for 1 h in order to convert $Gd(NO_3)_3$ and $Ce(NO_3)_3$ to the GDC phase.

Prior to the fabrication of LSCF electrode, Pt pastes were painted as counter electrode and reference electrode on the GDC electrolyte and sintered at 1000 °C for 1 h. The counter electrode was positioned symmetrically to the LSCF cathode and the reference electrode was fixed at the rim of the GDC electrolyte substrate. Two Pt meshes were attached to the working electrode (a pure LSCF cathode or a GDC-infiltrated LSCF cathode) and to the counter electrode as current collectors for the electrochemical measurement. Electrochemical impedance spectra of LSCF electrodes were measured in a frequency range of 0.1 Hz–100 kHz with a signal amplitude of 5 mV at temperatures between 650 °C and 750 °C with an electrochemical work station (Chi604D). The electrode polarization or area specific resistance was derived from the difference between the low and high-frequency intercepts at the real impedance axis.

Table 1
ICP analysis result of the LSCF obtained by the electrospinning method.

Nominal composition	Elemental composition			
	La	Sr	Co	Fe
$La_{0.8}Sr_{0.2}Co_{0.2}Fe_{0.8}O_{3-\delta}$	0.80	0.20	0.19	0.81

The microstructures of LSCF and GDC-infiltrated LSCF cathodes were analyzed by a scanning electron microscope.

3. Results and discussion

The ICP analysis result of the LSCF obtained by the electrospinning method is summarized in Table 1. Considering the experimental errors, we can confirm that the experimental composition for the sample match the nominal composition.

Fig. 1 shows the XRD pattern of electrospun LSCF nanofibers calcined at 900 °C for 2 h in air. As can be seen from Fig. 1, the sharp peaks indicate that the as-calcined nanofibers have a high crystalline characteristic. All the peaks can be indexed to a pure perovskite-type phase of LSCF.

SEM images of the as-spun LSCF/PVP nanofibers and of annealed LSCF nanostructured fibers are presented in Fig. 2. It can be seen that nanofibers with a long, smooth and uniform morphology have been successfully fabricated on a large scale in Fig. 2(a). The nanofibers are randomly distributed with a diameter of about 400 nm. Fig. 2(b) exhibits LSCF nanofibers calcined at 900 °C for 2 h. After calcination of the electrospun nanofibers, their texture changed from long nanofibers to short nanorods with diameters in the range of 200∼300 nm due to the thermal treatment process.

Some typical cross-sectional SEM images of the nanorod structured LSCF cathode and the nanoparticle structured LSCF cathode after the cell test are showed in Fig. 3. It can be observed that the nanorod structured LSCF cathode sintered at 940 °C is composed of unifom nanorods of 200–300 nm in diameter (Fig. 3a and b). The LSCF nanorods are randomly distributed in the cathode and poorly connected to each other, which results in high porosity. Fig. 3c and d shows SEM images of nanoparticle structured LSCF cathode calcined at 1000 °C. It can be seen that the LSCF cathode is well sintered with grain sizes in the range of 200–400 nm. Furthermore, there is good bonding among nanoparticles as well as good adhesion between cathode and electrolyte. But it has lower porosity compared to the nanorod structured LSCF cathode.

Impedance spectra of the nanorod structured LSCF cathode and nanoparticle structured LSCF cathode, measured at 650 °C

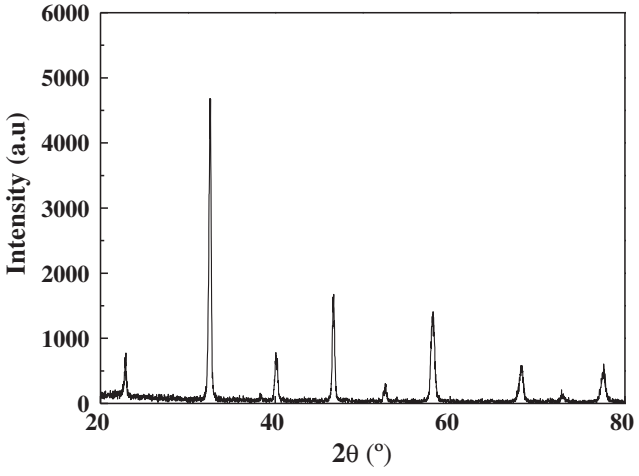

Fig. 1. XRD pattern of LSCF nanofibers being calcined at 900 °C for 2 h.

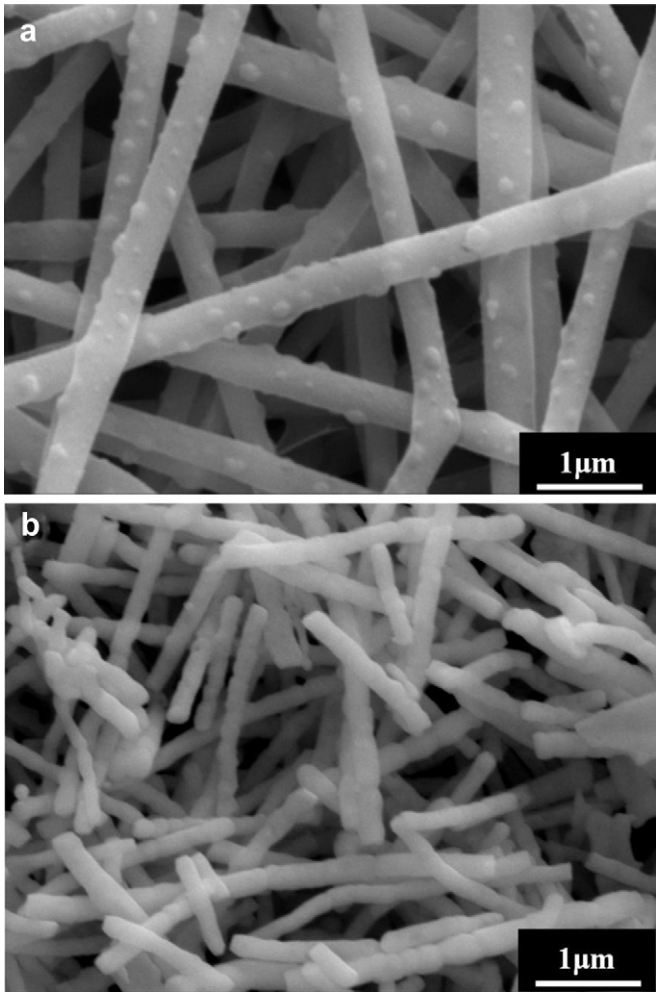

Fig. 2. SEM images of as-spun and calcined LSCF nanofibers: (a) as-spun fibers; (b) after calcined at 900 °C for 2 h.

and in open circuit conditions, are shown in Fig. 4. All the spectra were collected when the cell reached a stable state. The polarization resistances of LSCF cathodes can be calculated through the difference between the intercepts of the impedance arcs with the real axis at high frequencies and at low frequencies. In order to clearly show the difference in the electrode polarization behavior, the bulk resistances were removed from the spectra, showing only the cathode polarization impedances. As can be seen in Fig. 4a, the impedance spectrum for the nanorod structured LSCF cathode is composed of a high frequency capacitive arc and a low frequency capacitive arc. According to Leng et al. [31], the high frequency arc is due to the transfer of oxygen ions from the electrode into the electrolyte, while the low frequency arc is attributed to the oxygen dissociative adsorption and/or surface diffusion of oxygen species. The sum of the diameters of these two arcs is ascribed to the polarization resistance for the nanorod structured LSCF cathode, which is 14.12 Ω cm^2. As shown in Fig. 4b, compared with the nanorod structured LSCF cathode, the nanoparticle structured LSCF cathode only has a smaller impedance arc with a polarization resistance of 3.13 Ω cm^2, indicating a better electrochemical activity for O_2 reduction reactions. The difference of polarization resistances between nanorod structured LSCF cathode and nanoparticle structured LSCF cathode can be related to the size of the three-phase boundaries (TPB) where the O_2 reduction reactions take place. From Fig. 3a and c, it can be observed that the

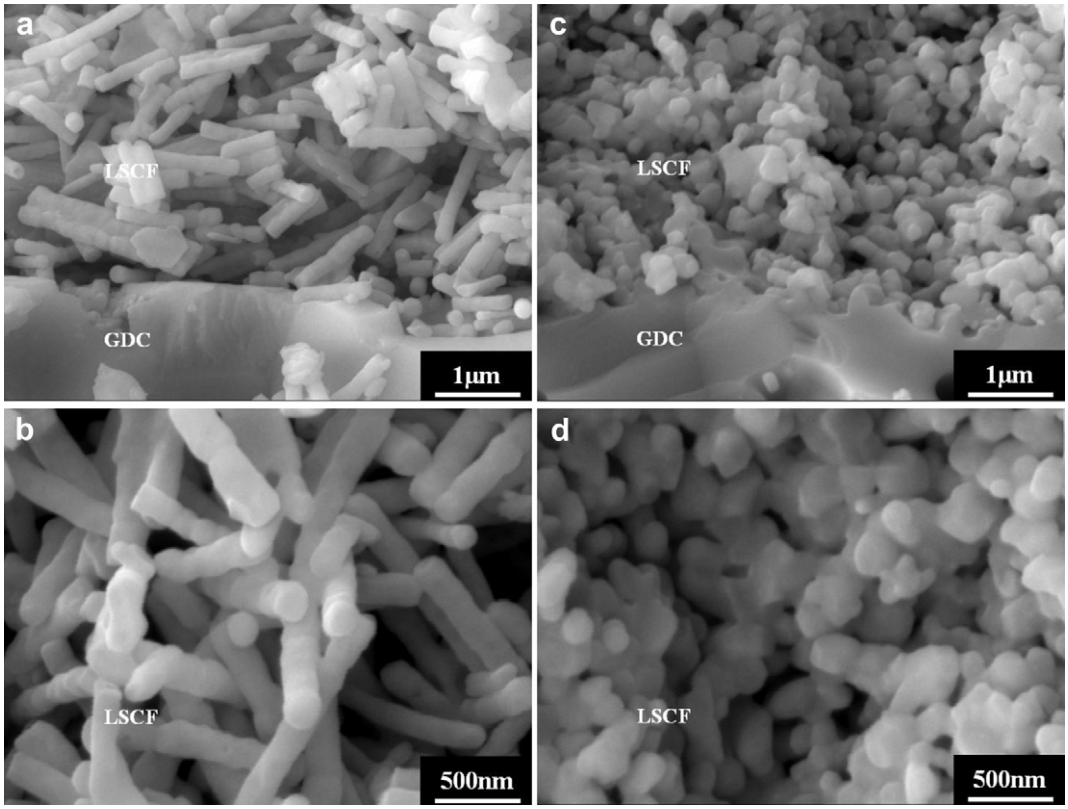

Fig. 3. SEM images of nanorod structured LSCF cathode calcined at 940 °C for 1min (a and b); SEM images of nanoparticle structured LSCF cathode calcined at 1000 °C for 2 h (c and d).

electrode/electrolyte contact area for the nanorod structured LSCF cathode is less than that of the nanoparticle structured LSCF cathode, resulting in a lower TPB length and a higher polarization resistance.

To increase the TPB length of the nanorod structured LSCF cathode, infiltration of GDC phase into LSCF cathode was developed. Fig. 5 shows the cross-sectional SEM images of GDC-infiltrated nanoparticle structured LSCF calcined at 800 °C for 1 h. For nanoparticle structured LSCF cathode, after infiltrated with 40 μL GDC precursor solution (Fig. 5a), the LSCF substrate got coarser and the grain boundaries became invisible, indicating that the newly formed GDC phases were coated on the surface of the LSCF substrate. As the infiltration loading of GDC was increased, more and more GDC phases appeared on the surface of the LSCF substrate so that the cathode became gradually denser, as shown in Fig. 5b–d.

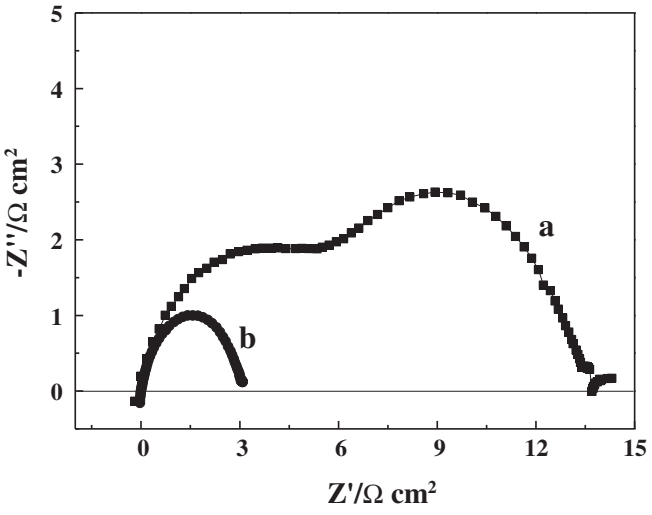

Fig. 4. Impedance spectra of nanorod structured LSCF cathode (a) and nanoparticle structured LSCF cathode (b) at 650 °C.

Fig. 6 shows the cross-sectional microstructures for GDC infiltrated nanorod structured LSCF cathodes fired at 800 °C for 1 h Fig. 6a is the SEM image of nanorod structured LSCF cathode infiltrated with 40 μL GDC precursor solution. It can be seen that some fine GDC nanoparticles appeared on the surface of LSCF nanorods. For the infiltrated nanorod structured LSCF cathode with 80 μL GDC solution, more GDC nanoparticles were coated on the surface of LSCF nanorods (Fig. 6b). When the GDC infiltration loading increased to 120 μL and 160 μL, the GDC infiltrated nanorod structured LSCF cathodes still keep one dimensional structures with high porosity, as shown in Fig. 6c and d. However, for the nanorod structured LSCF cathodes infiltrated with 200 μL and 240 μL GDC precursor solutions, the electrode porosity turns lower (shown in Fig. 6e and f).

The impedance spectra of GDC-infiltrated LSCF cathodes, measured at 650 °C in air and under open circuit conditions, are shown in Fig. 7. Prior to the GDC infiltration, the nanoparticle structured LSCF substrate was calcined at 1000 °C for 2 h and the nanorod structured LSCF skeleton was calcined at 940 °C for 1 min. In order to compare the difference of electrochemical activity of GDC-infiltrated LSCF cathodes with various infiltration loadings, all electrolyte ohmic resistances were removed from the impedance data. As can be seen in Fig. 7, the impedance arcs for GDC-infiltrated LSCF cathodes are much smaller than those for the blank LSCF cathodes (Fig. 4), mainly due to the enlargement of TPB which

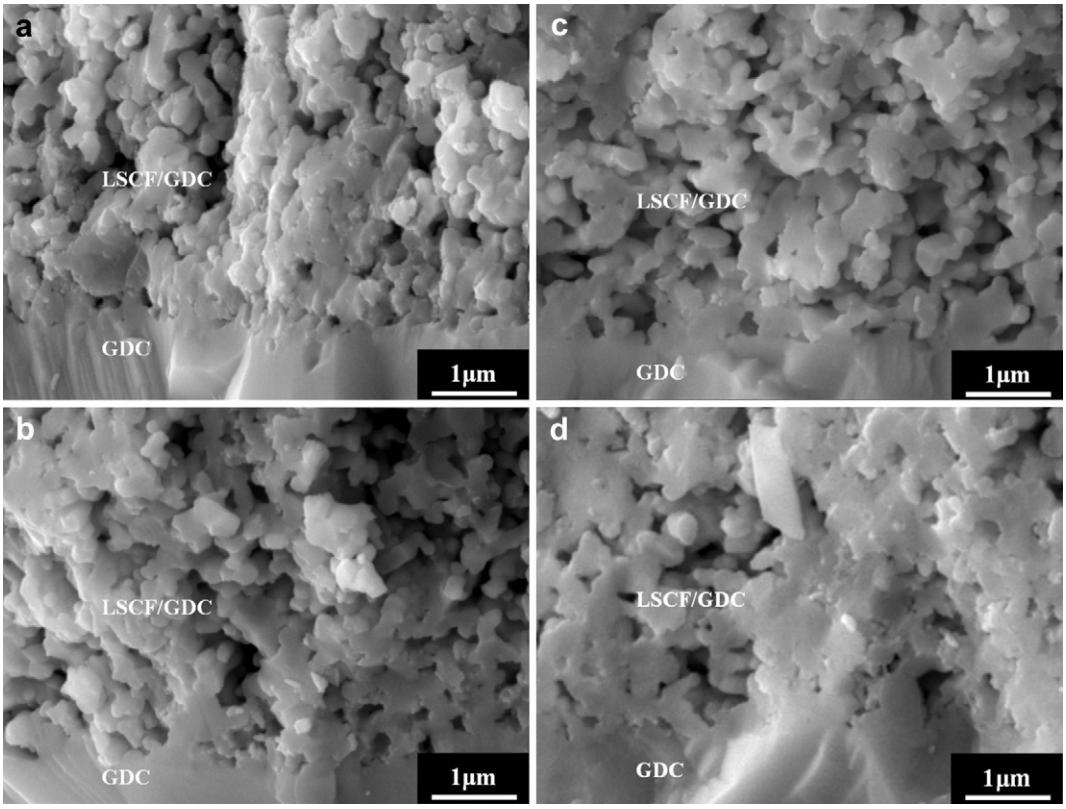

Fig. 5. The cross-sectional SEM images of nanoparticle structured LSCF cathodes infiltrated with GDC after electrochemical measurement as a function of the infiltration amount of GDC precursor solution: (a) 40 μL, (b) 60 μL, (c) 80 μL, and (d) 100 μL.

changed from a two-dimensional interface between the cathode and the electrolyte to an entire three dimensional cathode. The polarization resistances of GDC-infiltrated nanoparticle structured LSCF cathodes are reduced to 1.28, 0.87, 0.51 and 0.60 Ω cm^2 at 650 °C, respectively, for the infiltration of 40, 60, 80, 100 μL of 0.25 mol L^{-1} GDC precursor solutions into a nanoparticle structured LSCF substrate. In contrast, the infiltrated nanorod structured cathodes had a much better performance, and the polarization

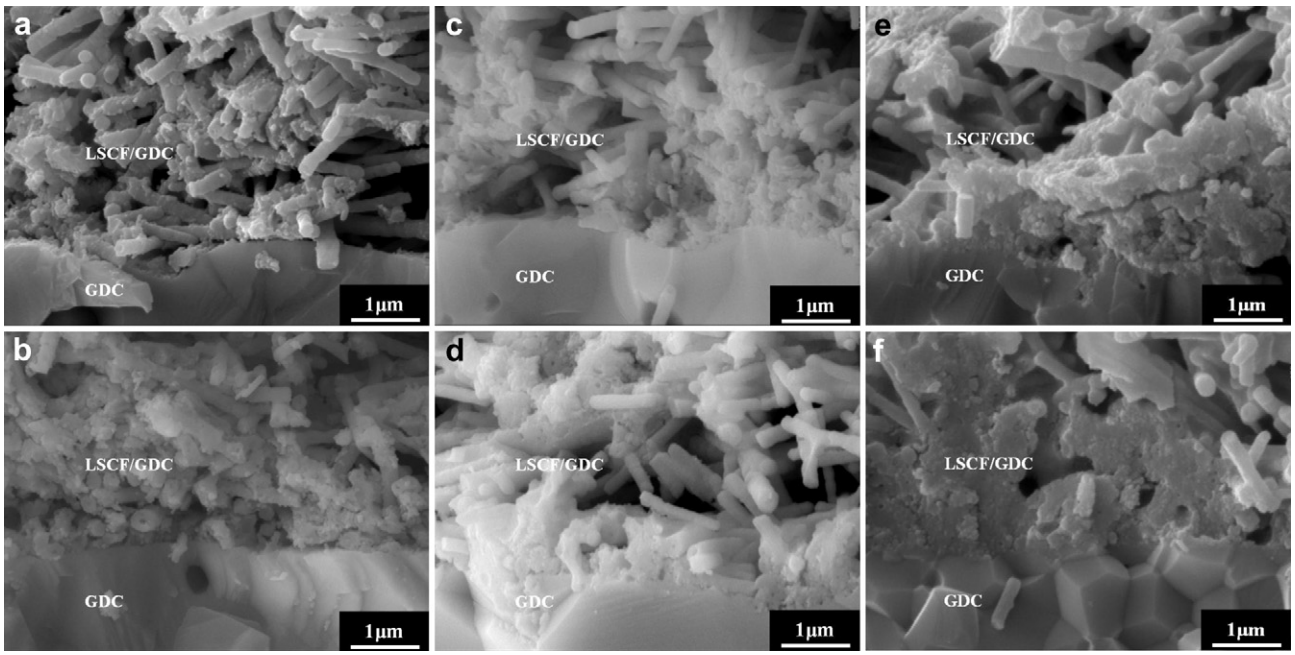

Fig. 6. The cross sectional SEM images of nanorod structured LSCF cathodes infiltrated with GDC after electrochemical measurement as a function of the infiltration amount of GDC precursor solution: (a) 40 μL, (b) 80 μL, (c) 120 μL, (d) 160 μL, (e) 200 μL and (f) 240 μL.

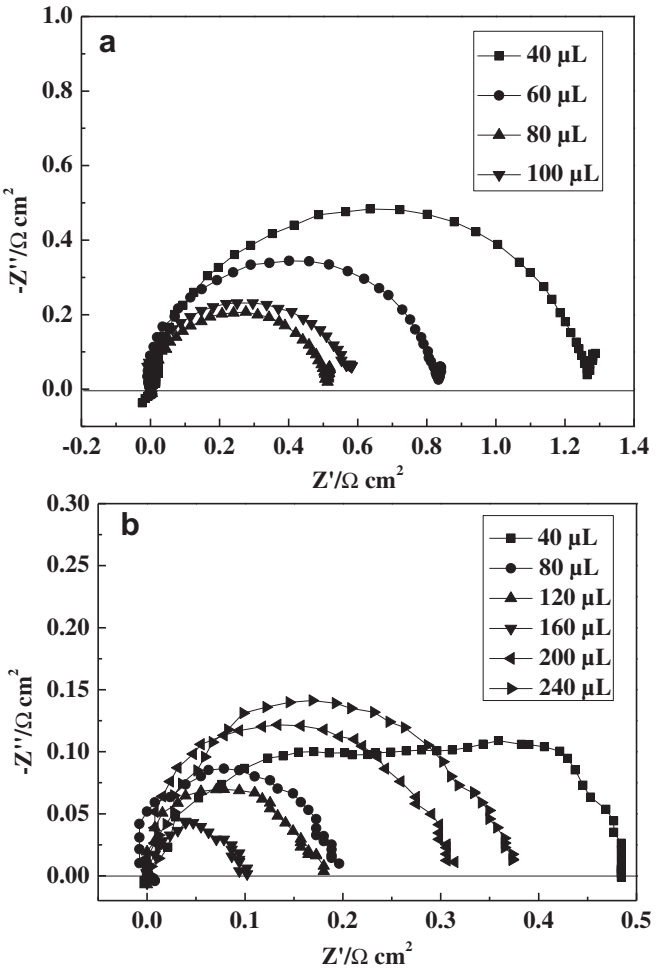

Fig. 7. Electrochemical impedance spectra of GDC-infiltrated LSCF composite cathodes versus the infiltration amount of GDC: (a) infiltrated nanoparticle structured LSCF cathodes; (b) infiltrated nanorod structured LSCF cathodes.

resistances at 650 °C for infiltrated nano-rod structured cathodes with 40 μL, 80 μL, 120 μL, 160 μL, 200 μL and 240 μL GDC solutions are 0.49, 0.20, 0.18, 0.10, 0.31, 0.37 Ω cm^2, respectively. The excellent electrochemical performance of GDC-infiltrated nanorod structured LSCF cathodes is ascribed to large LSCF/GDC boundaries and proper porosity. From Fig. 5d, the infiltrated nanoparticle structured LSCF cathode with 100 μL GDC solution has a very dense microstructure, which blocks the gas diffusion, decreases the TPB length, and thus results in a higher polarization compared to that of 80 μL GDC-infiltrated nanoparticle structured LSCF cathode. This similar phenomenon also occurs on the GDC-infiltrated nanorod structured LSCF cathodes. But the nanorod structured LSCF cathode infiltrated with 160 μL GDC still retain higher porosity (Fig. 6d), which facilitates the gas-phase diffusion process and contributes to a lower polarization resistance. As shown in Fig. 7b, it is interesting that the low frequency arc of the impedance spectrum for nanorod structured LSCF cathode vanishes gradually with the increase in TPB size caused by the infiltration of GDC phase into the pores of nanorod structured LSCF cathode. We believe that this phenomenon is exactly the evidence for the origination of the low frequency arc from the surface adsorption and surface diffusion processes of oxygen species.

Therefore, it is demonstrated that the electrochemical performance of nanorod structured LSCF cathode can be significantly enhanced by infiltration of the GDC phase into a nanorod structured LSCF scaffold pre-sintered in 940 °C; the cathode polarization resistance is reduced from 14.12 to 0.10 Ω cm^2. It is noted that polarization resistance of the infiltrated nanorod structured LSCF cathode shows 5 times smaller than that of the infiltrated nanoparticle structured LSCF cathode under the identical testing conditions, however, the weight of LSCF nanorod substrate is only 0.5 times that of LSCF nanoparticle substrate. For the nanorod structured cathode infiltrated with 160 μL GDC solution, the polarization resistance of 0.10 Ω cm^2, which is lower than those of other LSCF composite cathodes (Table 2) reported in the literature [12,16,17,24,32,33]. These results show that the nanorod structured LSCF cathode infiltrated with GDC nanoparticles is a promising cathode material for IT-SOCFs.

Table 2
Comparison of the polarization resistances (R_p) for LSCF composite cathodes, measured at 650 °C.

Cathode	R_p (Ω cm^2)	References
LSCF/GDC	0.10	Present work
LSCF/GDC	0.52	Fu et al. [12]
LSCF/SDC	0.40	Nie et al. [16]
LSCF/GDC	0.45	Chen et al. [17]
LSCF/SSC	0.12	Lou et al. [24]
LSCF/SDC	0.265	Lee et al. [32]
LSCF/YSZ	0.218	Chen et al. [33]

4. Conclusions

One dimensional LSCF/GDC nanocomposite prepared by electrospinning technique and a multi-step infiltration process has been demonstrated to be a good candidate as IT-SOFC cathodes. For the nanorod structured LSCF cathode infiltrated with 40 μL, 80 μL, 120 μL and 160 μL of GDC precursor solution, the polarization resistances are 0.49, 0.20, 0.18 and 0.10 Ω cm^2 at 650 °C, respectively. It is worth noting that polarization resistance of the nanorod structured LSCF/GDC cathode with 160 μL GDC loading shows 5 times smaller than that of LSCF/GDC nanoparticle composite cathode with the optimal GDC loading of 80 μL under the identical testing conditions, which is attributed to its excellent structure with larger LSCF/GDC boundaries length and higher porosity. To further improve the electrochemical performance of LSCF/GDC nanocomposite cathode, we will further optimize the microstructures of one dimensional LSCF cathode in the future.

Acknowledgments

This work is funded by National Natural Science Foundation of China (51072040), National Program on Key Basic Research Project (973 Program 2012CB215400), and the National Science Foundation of China (Grant No. 51172275).

References

[1] M.F. Liu, D.H. Dong, R.R. Peng, J.F. Gao, J. Diwu, X.Q. Liu, G.Y. Meng, J. Power Sources 180 (2008) 215–220.
[2] J.M. Wang, Z. Lü, X.Q. Huang, K.F. Chen, N. Ai, J.Y. Hu, W.H. Su, J. Power Sources 163 (2007) 957–959.
[3] B.C.H. Steele, Solid State Ionics 129 (2000) 95–110.
[4] K.R. Reddy, K. Karan, J. Electroceram. 15 (2005) 45–56.
[5] A. Mai, V.A.C. Haanappel, S. Uhlenbruck, F. Tietz, D. Stover, Solid State Ionics 176 (2005) 1341–1350.
[6] L.d. Conceição, A.M. Silva, N.F.P. Ribeiro, M.M.V.M. Souza, Mat. Res. Bull. 46 (2011) 308–314.
[7] S.P. Jiang, Solid State Ionics 146 (2002) 1–22.
[8] M.L. Liu, J. Electrochem. Soc. 145 (1998) 142–154.
[9] J. Fleig, J. Power Sources 105 (2002) 228–238.
[10] X.Y. Lou, Z. Liu, S.Z. Wang, Y.H. Xiu, C.P. Wong, M.L. Liu, J. Power Sources 195 (2010) 419–424.

[11] C.W. Sun, R. Hui, J. Roller, J. Solid State Electrochem. 14 (2010) 1125–1144.
[12] Q. Fu, K.N. Sun, N.Q. Zhang, X.D. Zhu, S.R. Le, D.R. Zhou, J. Power Sources 168 (2007) 338–345.
[13] V. Dusastre, J.A. Kilner, Solid State Ionics 126 (1999) 163–174.
[14] S.P. Jiang, Y.J. Leng, S.H. Chan, K.A. Khor, Electrochem. Solid-State Lett. 6 (2003) A67–A70.
[15] F. Zhao, Z.Y. Wang, M.F. Liu, L. Zhang, C.R. Xia, F.L. Chen, J. Power Sources 185 (2008) 13–18.
[16] L.F. Nie, M.F. Liu, Y.J. Zhang, M.L. Liu, J. Power Sources 195 (2010) 4704–4708.
[17] J. Chen, F.L. Liang, B. Chi, J. Pu, S.P. Jiang, J. Li, J. Power Sources 194 (2009) 275–280.
[18] M. Shah, S.A. Barnett, Solid State Ionics 179 (2008) 2059–2064.
[19] A. Dutta, J. Mukhopadhyay, R.N. Basu, J. Eur. Ceram. Soc. 29 (2009) 2003–2011.
[20] Y.J. Leng, S.H. Chan, Q.L. Liu, Int. J. Hydrogen Energy 33 (2008) 3808–3817.
[21] Y.M. Kim, S.W. Baek, J. Bae, Y.S. Yoo, Solid State Ionics 192 (2010) 595–598.
[22] B.a. Fan, X.L. Liu, Solid State Ionics 180 (2009) 973–977.
[23] C.J. Fu, K.N. Sun, N.Q. Zhang, X.B. Chen, D.R. Zhou, Electrochim. Acta 52 (2007) 4589–4594.
[24] X.Y. Lou, S.Z. Wang, Z. Liu, L. Yang, M.L. Liu, Solid State Ionics 180 (2009) 1285–1289.
[25] W.H. Kim, H.S. Song, J. Moon, H.W. Lee, Solid State Ionics 177 (2006) 3211–3216.
[26] W.G. Wang, M. Mogensen, Solid State Ionics 176 (5–6) (2005) 457–462.
[27] A.M. Azad, T. Matthews, J. Swary, Mater. Sci. Eng. B 123 (2005) 252–258.
[28] L.P. Li, P.G. Zhang, R.R. Liu, S.M. Guo, J. Power Sources 196 (2011) 1242–1247.
[29] M.J. Zhi, S. Lee, N. Miller, N.H. Menzler, N.Q. Wu, Energy Environ. Sci. 5 (2012) 7066–7071.
[30] R.O. Fuentes, R.T. Baker, J. Power Sources 186 (2009) 268–277.
[31] Y.J. Leng, S.H. Chan, K.A. Khor, S.P. Jiang, Int. J. Hydrogen Energy 29 (2004) 1025–1033.
[32] S. Lee, H.S. Song, S.H. Hyun, J. Kim, J. Moon, J. Power Sources 195 (2010) 118–123.
[33] J. Chen, F.L. Liang, L.N. Liu, S.P. Jiang, B. Chi, J. Pu, J. Li, J. Power Sources 183 (2008) 586–589.